Int J Adv Manuf Technol (2013) 65:433–441
DOI 10.1007/s00170-012-4182-4

ORIGINAL ARTICLE

Form error compensation in single-point inclined axis nanogrinding for small aspheric insert

Fengjun Chen · Shaohui Yin · Hitoshi Ohmori · Jianwu Yu

Received: 15 November 2011 / Accepted: 17 April 2012 / Published online: 31 July 2012

Abstract Based on an examination of traditional arc-enveloped grinding method, a single-point inclined axis nanogrinding method is presented to grind an aspheric insert by compensating tool setting error, radius error, and residual form error. Profile data from on-machine measurement are used to obtain the tool setting error and radius error of grinding wheel, as well as the normal residual form error. Compensation method of single-point inclined axis nanogrinding is built up for generating new compensation path. Grinding test of aspheric tungsten carbide insert with diameter 9.5 mm is conducted to evaluate performances of the grinding mode and compensation method. A last form error of 200 nm in peak to valley and surface roughness of 2.243 nm in Ra are achieved. These results indicated that the form error compensation method and single-point inclined axis nanogrinding mode can significantly improve form accuracy and surface roughness of ground surface.

Keywords Error compensation · Wheel setting error · Radius error · Residual error · Single-point inclined axis grinding · Aspheric insert

F. Chen · S. Yin (✉) · J. Yu
National Engineering Research Center for High Efficiency Grinding, Hunan University,
Changsha 410082, People's Republic of China
e-mail: shyin2000@hotmail.com

H. Ohmori
The Institute of Physical and Chemical Research (RIKEN),
Saitama 351-0198, Japan

1 Introduction

Recent years witnessed increasing demand for high-quality optoelectronic components in optical instruments and astronautics fields [1, 2]. High-performance CNC machine tools and high-efficiency manufacturing technologies have to be continuously improved to meet the need [3]. Ultra-precision machining has drawn much attention and nanogrinding has been extensively used for machining brittle and hard materials [4–7]. The error compensation is an essential issue for improving the machining accuracy, which is affected by some error sources such as geometric error of machine tools, tool deflection, wear error, and thermal error [8, 9]. It is efficient and less expensive to improve machining accuracy and surface quality of workpiece via modifying NC program for next compensation cycle.

The geometric errors can be compensated by building geometrical error model of machine tools. Liang et al. [10] developed a comprehensive error compensation system to correct 11 geometric error components on a turning center. Lei and Sung [11] proposed the setting NURBS path to approximate its error compensation function and to generate a new compensated path. Uddin et al. [12] presented a simulator of geometric errors in five-axis machine tool by considering kinematical errors. Khan and Chen [13] described an efficient correction methodology to compensating the overall effect of all position-dependent- and position-independent errors. Thermal errors are induced by a spindle, linear motors, bearings, and ambient temperature in precision machining. Various thermal error models have been built based on different compensation methods [14, 15].

In tool wear and deflect respects, Zhang et al. [16] presented an evaluation method of the wheel's wear based on digital image acquisition. Rahman et al. [17] compensated the wheel wear until the profile error reaches within

tolerable limit in ELID grinding of an aspheric surface. Suzuki et al. [18] studied on the tool errors and its compensation methods in precision grinding of micro aspheric surface. Lee et al. [19] corrected the form error derived from tool de-centring in the ultra-precision machining of aspheric surfaces. Habibi et al. [20] developed appropriate tool deflection estimation model and complementary algorithms for compensation of these errors.

Some compensated methods based on the residual error of ground workpiece have also been reported [21, 22]. Most of recently developed solutions cannot fulfill workshop needs and are limited to research papers. In the present study, an error compensation method based on a single-point inclined axis grinding mode is proposed for correcting wheel position and generating the new tool path in grinding aspheric insert. The tool setting error in *X* and *Y* axes and radius error of grinding wheel are considered. The normal residual error is taken into account for next compensation grinding. To verify the proposed grinding mode and compensation approach, a nanogrinding test is conducted for the fabrication of a small aspheric tungsten carbide insert.

2 Single-point inclined axis grinding mode

The schematic diagram of four-axis ultra-precision nanogrinding and on-machine measurement is shown in Fig.1. In this mode, the workpiece spindle may linearly move along *Y*–*Z*-axis. Grinding spindle is installed on *B*-axis rotary table which can linearly move with on-machine measurement system on *X*-axis table [22]. After grinding, the workpiece needs not to be uninstalled and can be measured directly on the machine. A micro ruby measuring probe is driven along the measuring path and contacts with the measured surface under a certain pressure. The deviation signals from high-precision displacement sensors are transferred to PC for data processing. It should be noted that the on-machine measuring method can avoid reinstallation error, improve machining efficient and compensation accuracy and make operation easy to use.

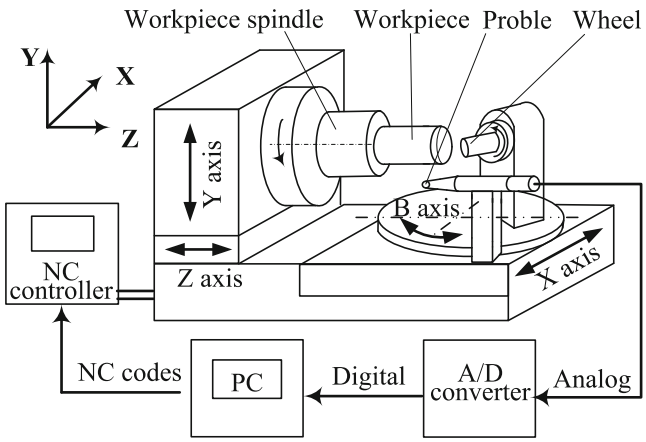

Fig. 1 Schematic diagram of nanogrinding and on-machine measurement

As is shown in Fig. 2a, the arc-enveloped grinding mode is usually used for grinding aspheric surface. In this conventional method, the axial direction of arc grinding wheel remains constant and the different grinding points of arc grinding wheel contacts with ground surface. Point A_1 on the grinding wheel contacts with the point P_1 of the workpiece surface, and point A_2 on the grinding wheel contacts with the point P_2 of workpiece surface. This mode can average the wear loss and prolong the life of grinding wheel during grinding large surface. However, it is limited to the shape of ground surface and the dimension of grinding wheel, and the arc profile of grinding wheel is difficult to be trued and dressed. When grinding a small aspheric surface, the wear of the grinding wheel is relatively smaller compared to the case when grinding a large surface.

In order to solve the above problem, a single-point inclined axis grinding mode is employed for grinding small aspheric surface in Fig. 2b. In the new grinding mode, grinding wheel rotates around the *B*-axis and keeps the same grinding tip point of grinding wheel in different grinding areas of aspheric surface. As is shown in Fig. 2b, the tip point A_2 of the grinding wheel contacts with the workpiece surface at point P_1. When grinding the point P_2, the grinding wheel rotates from the angle α_1 to the angle α_2 around the *B*-axis and makes the same tip point A_2 contact at point P_2 with the same posture. The new grinding mode can avoid the interference while grinding small aspheric insert and make the controlling of *B*-axis very easy. In addition, the truing and dressing of end face and cylindrical surfaces of grinding wheel are easy to obtain the new grinding tip.

3 Error analysis in single-point inclined axis grinding

3.1 Error types of grinding wheel in *X*-axis

In general, initial setting positions of grinding wheel and workpiece must be adjusted manually before grinding. However it is difficult to obtain a very precise setting position. The setting error of grinding wheel in *Y*-axis may result in the offset of the ground profile and generate a navel at the center of ground surface.

Figure 3 illustrates the different profiles of actual ground surface due to different error types of grinding wheel along *X*-axis. There are two types of setting error, namely "inward offset" and "outward offset" along *X*-axis commonly encountered in nanogrinding. Inward offset means the setting position does not reach the ideal grinding center, and outward offset means that the tool setting position has passed it.

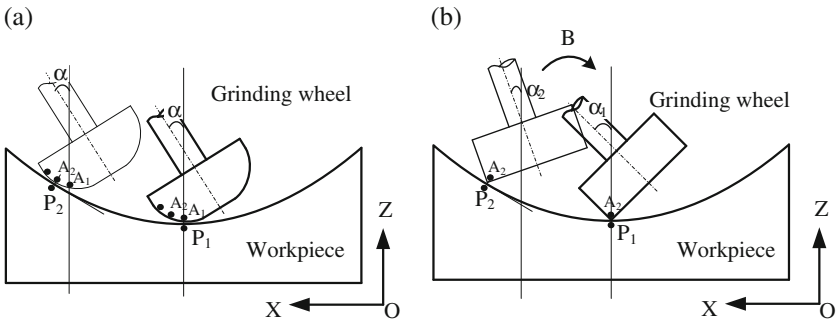

Fig. 2 **a** Arc-enveloped grinding mode and **b** single-point inclined axis grinding mode

The tool setting error can result in an approximate "V-shaped" or "Λ-shaped" error profile. A Λ-shaped error profile will be generated when the setting error of the grinding wheel is outward for a concave surface (Fig. 3a) and the setting error is inward for a convex surface (Fig. 3d). Likewise, an approximate V-shaped error profile can be measured when the setting error of the grinding wheel is inward for a concave surface (Fig. 3b) and the setting error is outward for a convex surface (Fig. 3c). The wheel setting error can be distinguished by analyzing the profile shape of ground surface.

3.2 Setting error of grinding wheel in *X*-axis

Initial form error resulted from setting error of grinding wheel should be removed at the first step of error compensation. For example, a V-shaped error profile of concave surfaces is considered for computing the outward setting error of grinding wheel. Figure 4 shows the relationship of the setting error of grinding wheel with the form error on concave spherical and aspheric surfaces, respectively. e_i is a measured form error at arbitrary point T_i, r is the radius of spherical surface in Fig. 4a, x_i is the *X*-axis coordinate value at point T_i, and *ex* is a setting error of grinding wheel which can be computed by:

$$ex = x_i - \sqrt{r^2 - \left(\sqrt{r^2 - x_i^2} + e_i\right)^2} \tag{1}$$

If the ground workpiece is an aspheric surface shown in Fig. 4b, the setting error of a grinding wheel can also be computed by:

$$F(x_i - \mathrm{ex}) + e_i = F(x_i) \tag{2}$$

Where $F(x)$ is a formula of aspheric surface. According to the Newtonian iteration, the setting error ex at point T_i can be obtained by iteratively calculating Eq. 2. After fitting these measured data, several calculation points should be chosen away from the center of error profile and then be averaged to get the accurate setting error of grinding wheel for compensation grinding.

Figure 5 shows the relationship between the form error e_i and the setting error ex when the apertures of workpiece are 5 and 10 mm, respectively. When the setting error becomes larger, the residual error of ground workpiece will increase. The residual error remains unchanged when the setting error is same, regardless of the change in the ground aperture of workpiece. The wheel setting error in the *X*-axis will result in obvious form error.

3.3 Setting error of grinding wheel in *Y*-axis

According to grinding mode, if the grinding wheel cannot be precisely positioned at the center of the workpiece in *Y*-axis, two kinds of setting errors will occur as shown in Fig. 6. The setting errors in *Y*-axis include the positive and

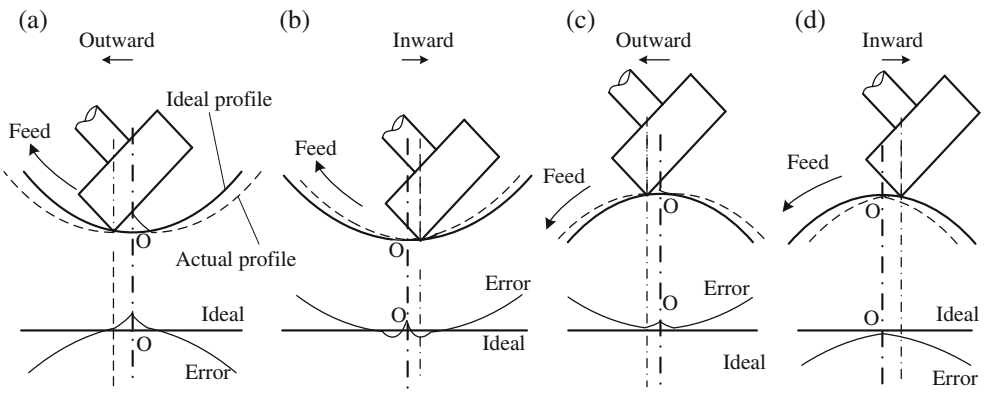

Fig. 3 Different profile types of wheel setting error in *X*-axis including **a** outward offset and **b** inward offset of concave surface; **c** outward offset and **d** inward offset of convex surface

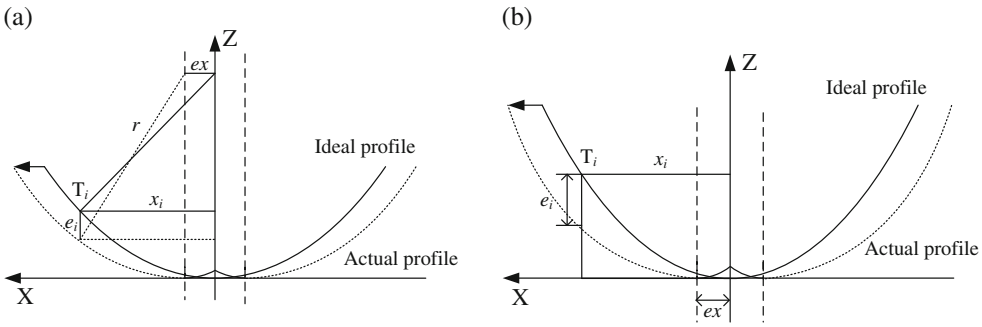

Fig. 4 Calculation of wheel setting error of **a** spherical surface and **b** aspheric surface

the negative deviations. Because of the rotational symmetry of the aspheric surface, the errors cannot be determined only from the residual shape of the ground surface.

In general, the rotation speed of grinding wheel is much greater than that of the workpiece. Figure 6a shows that the relative speed at grinding point is the resultant speed of the wheel and workpiece, which makes the grinding traces of abrasives appear counterclockwise vortex. Near the center of the workpiece in particular, the rotational speed of the workpiece is very low, so the abrasive scratches are more apparent. Therefore, when the setting error of the grinding wheel is positive in *Y*-axis, the vortex-like grinding traces appear counterclockwise at edge of the center ridge. Similarly, when the setting error of the grinding wheel is negative and the grinding traces at the center are shown in Fig. 6b.

Setting errors of the grinding wheel in *Y*-axis will also result in larger-than-ideal grinding range and cutting depth. As is shown in Fig. 7, the ideal grinding path in *XOY* plane is $OC_1B_1A_1$. Because of the positive error of the grinding wheel, the actual grinding path is along *CBA* though the workpiece still rotates around the center point O. When the grinding wheel arrives at point B, the actual grinding amount is the same as the point B_1. *D* is the grinding aperture, and *d* is the setting error in *Y*-axis. When the grinding wheel grinds at point C, it reaches the center of the workpiece in *X*-axis, and the actual grinding point arrives at point C_1. The central region of the workpiece cannot be ground at $x<d$. The relationship between the cutting depth error ΔZ can be expressed as:

$$\Delta Z = F(x) - F\left(\sqrt{x^2 - (D/2)^2}\right);\ d \le x \le D/2 \tag{3}$$

On the other hand, the setting error of the grinding wheel in *Y*-axis will increase the grinding range of the workpiece:

$$\Delta X = \sqrt{(D/2)^2 + d^2} - D/2 \tag{4}$$

3.4 Radius error of grinding wheel

The radius error of the grinding wheel is an important factor in ultra-precision error compensation grinding. Suzuki et al. [18] only considered an approximate method for calculating the wheel radius error. However it is better to be precisely calculated in nanogrinding. As is shown in Fig. 8a, after worn, the actual radius of the grinding wheel is smaller than the ideal radius while grinding a concave spherical workpiece. The ideal profile and processing path of grinding wheel are expressed by the dashed curve, while the actual profile and processing path are expressed by solid curve. According to the geometric relationship in OAB, the equation can be given:

$$(R - \Delta R)^2 = (x_i)^2 + (R - \Delta R - h - \Delta h)^2; \tag{5}$$

$$h = R - \sqrt{R^2 - x_i^2}$$

where *R* is a spherical radius of workpiece, ΔR is the radius error of grinding wheel, and Δh is the deviation error between actual and ideal grinding profiles at X_i point, i.e., the measured value. By simplifying the

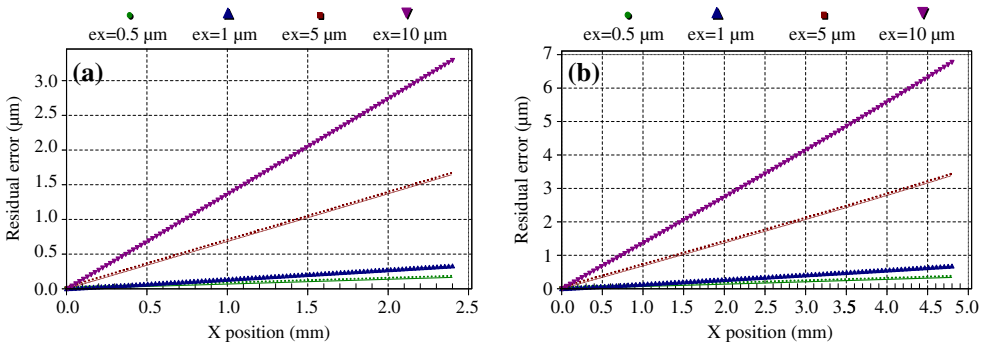

Fig. 5 Relationships of form error and wheel setting error. Grinding apertures of workpeice are **a** 5 mm and **b** 10 mm

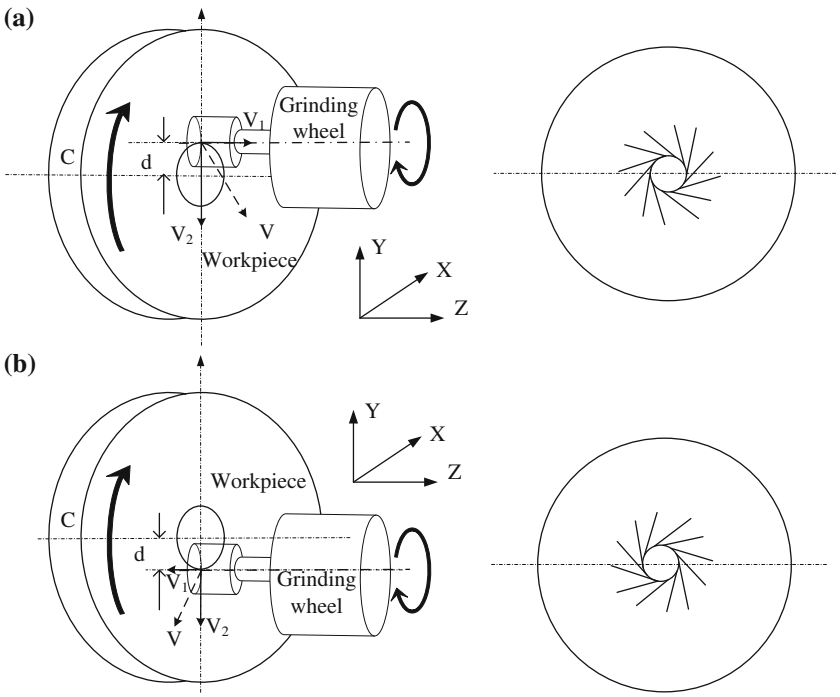

Fig. 6 **a** Positive error and **b** negative error of grinding wheel in *Y*-axis

above equation, the relationship of radius error of the grinding wheel and the measured error can be given by:

$$\Delta h = R - \Delta R - h - \sqrt{(R - \Delta R)^2 - x_i^2} \tag{6}$$

Figure 9 shows the relationship between the residual error and the radius error in grinding spherical surface. Residual error increases with the increase of radius error. When the aperture of workpiece changes, the residual error caused by the radius error shows similar tendency. When the aperture of workpiece becomes larger, the residual error is smaller for the same radius error in the same grinding place.

4 Error compensation protocol

Based on single-point inclined axis grinding, a protocol of compensation grinding is shown in Fig. 10. After initial fine grinding, an on-machine measurement system was used to measure the form accuracy of ground mold. If form error (peak to valley; PV) is obvious due to the setting error, it should be first compensated through resetting the center position of the grinding wheel. After eliminating setting error, residual error will be further processed to

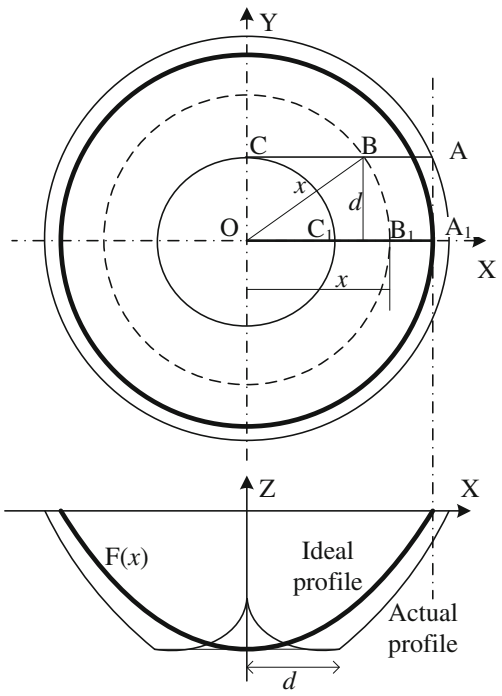

Fig. 7 Form error caused by setting error of grinding wheel in *Y*-axis

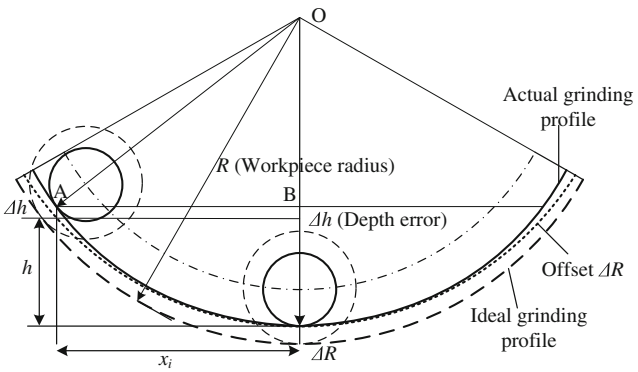

Fig. 8 Calculation of radius error of smaller radius

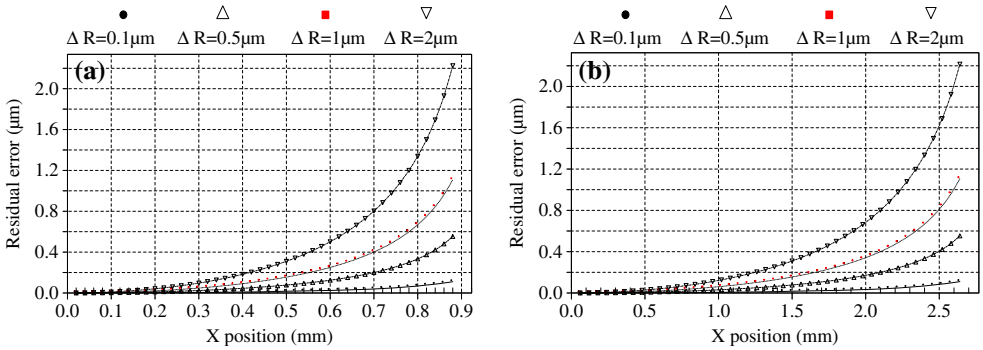

Fig. 9 Relationships of residual error and the radius error of grinding wheel for grinding spherical surface. Apertures of workpiece are **a** 2 mm and **b** 6 mm

generate new compensation path. Because the measured profile error data obtained from on-machine measurement contain high-frequency signals, it cannot be directly used and must be filtered to remove roughness noise. A normal residual error was calculated for compensating the profile error in normal direction [22]. Using this method, the actual path of measuring probe was first generated by superposing the processed profile error data on the original probe path. And then, the actual ground profile was obtained by subtracting the probe radius from the contact point along its normal direction. The normal residual error could be calculated by subtracting the target profile from the actual ground profile in the normal direction of ideal profile. The grinding wheel has to move a corresponding residual error in normal direction in order to compensate the residual error. New NC program and measuring program are generated and transferred to NC controller to drive the movement of axes. If the form accuracy of ground surface met the requirement, the compensation grinding would be terminated. Otherwise, new residual errors are calculated and compensation path is generated again and new compensation grinding is continuously conducted until the qualified form accuracy is obtained.

5 Error compensation of single-point inclined axis grinding

5.1 Experimental apparatus

A nanogrinding experiment was conducted on a four-axis ultra-precision machine by using above error compensation approaches. An on-machine contact measurement system was integrated by NACHI installed in this ultra-precision machine tool. The resolution is 1 nm, and the straightness accuracy is below 0.20 μm/300 mm. The radius of the measuring probe is 0.25 mm. The contact force is 0.53 N and the measuring angle is ±60 °. It has the same position accuracy as the ultra-precision machine tool. The external view of ultra-precision machine is shown in Fig. 11. It is suitable to grinding small size insert of diameter below 10 mm in diameter using single-point inclined axis mode. Tungsten carbide was used as the material of insert in this

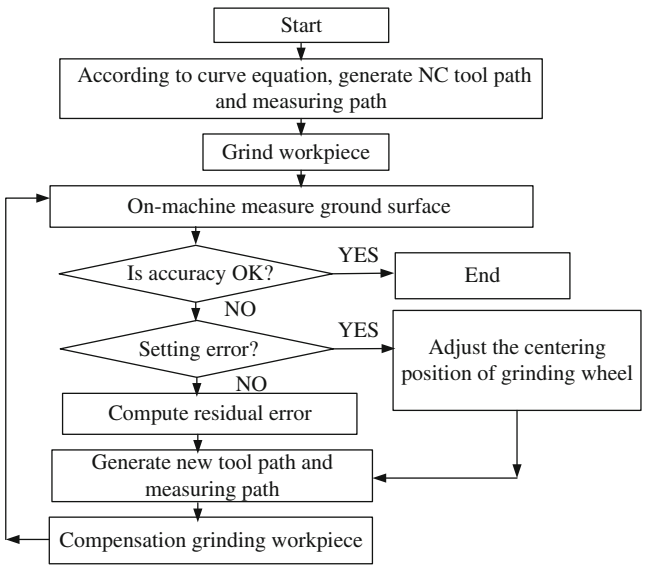

Fig. 10 Flow chart of compensation grinding

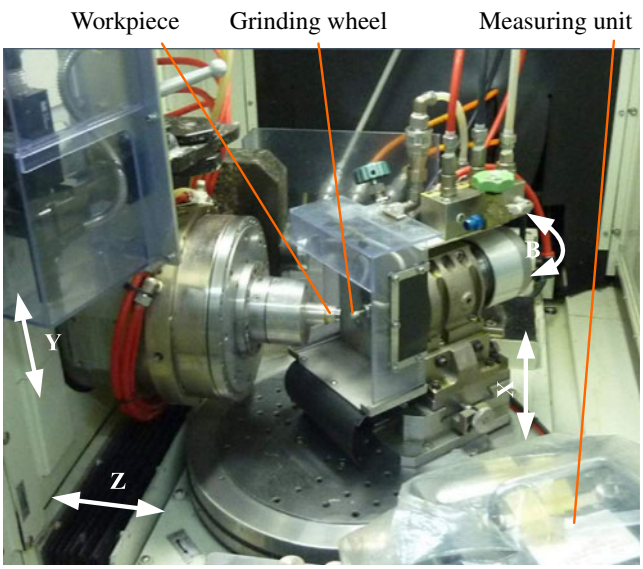

Fig. 11 External view of four-axis nanogrinding machine

test, and the aperture was 9.5 mm. A cylindrical grinding wheel was employed to grind a concave aspheric surface in a single-point inclined axis mode. The aspheric equation and some geometric parameters of insert are expressed:

$$z = \frac{x^2}{R\left(1+\sqrt{1-(1+K)x^2/R^2}\right)} + A_4x^4 + A_6x^6 + A_8x^8 + A_{10}x^{10} \quad (7)$$

where, R=22.2652 mm, K=−8.337661, A_4=3.77259e-05, A_6=2.75022e-07, A_8=−1.18687e-09, and A_{10}=2.28851e-011.

In this experiment, initial NC program of grinding path was generated and then transferred to ultra-precision machine for initially grinding the workpiece. After on-machine precision truing, #325 grinding wheel (cast iron bond) was first used for rough grinding so an aspheric surface was obtained high-efficiently. Subsequently #2000 grinding wheel (resin bond) was used for fine grinding and compensation grinding. Table 1 summarizes the grinding conditions.

5.2 Experiment results and discussions

After rough grinding by #325 grinding wheel and on-machine measurement indicated that a form accuracy of 588 nm in PV and 126 RMS were obtained in Fig. 12a. After fine grinding by #2000 grinding wheel and on-machine measurement showed that a form accuracies of 1,118 nm in PV and 368 nm in RMS were obtained after original (first) fine grinding cycle without compensation (shown in Fig. 12b). The Λ-shaped of error profile was obvious, and the setting type of grinding wheel was outward. Because of a great influence on the form accuracy, it should be first eliminated for next form error compensation. The value of setting error of 7.461 μm was calculated according to the Λ-shaped of error profile, and new center position of grinding wheel was reset. After second fine grinding, the form accuracy

Table 1 Rough and fine grinding conditions of aspheric insert

Grinding wheel	Rough grinding	Fine grinding			
	#325 (cast iron)	#2000 (resin)			
		1st	2nd	3 rd	4th
Cutting depth (μm)	2	1		0.5	
Feed rate (mm/min)	5	5		0.5	
Work rotation (rpm)	200	200			
Wheel rotation (rpm)	45,000	45,000			

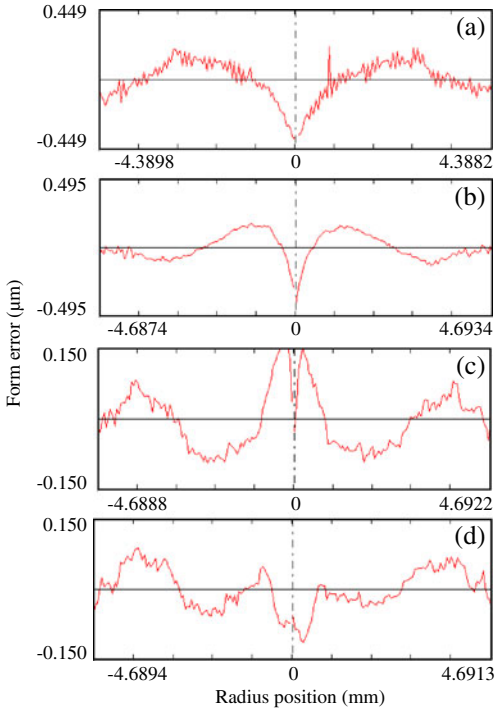

Fig. 12 Form accuracy after **a** rough grinding PV at 588 nm, RMS 126 nm; **b** first fine grinding PV 1,118 nm, RMS 368 nm; **c** second fine grinding PV 587 nm, RMS 99 nm; **d** third fine grinding PV 263 nm, RMS 63 nm; and **e** fourth fine grinding PV 200 nm, RMS 44 nm measured by on-machine measurement

was improved to PV at 587 nm and RMS 99 nm in Fig. 12c. The setting error of grinding wheel was basically eliminated, but the fluctuation of PV profile was obvious, especially the large navel in the center. It needed to be compensated by form error compensation, namely, these measured data were processed for compensating the form error and generating new path of grinding wheel. After third fine grinding and on-machine measurement, form accuracy was improved to PV at 263 nm and RMS 63 nm in Fig. 12d. To further improve the form accuracy, the compensation ratio of form error was set at 70 %. After fourth grinding cycle, form accuracy was improved to PV at 200 nm and RMS 44 nm in Fig. 12e.

It should be noted that the form accuracy of the first fine grinding were worse than those obtained after the rough grinding. This is mainly because the setting error had to also be compensated and the form accuracy was good when high-efficiently obtaining aspheric surface by #325 rough grinding wheel. The setting error would exist after installing fine grinding wheel for the first fine grinding. However, the surface roughness after rough grinding was worse than those obtained after finish grinding.

Because of ambient environment condition, a periodic wave appeared to be superposed on the ground profile

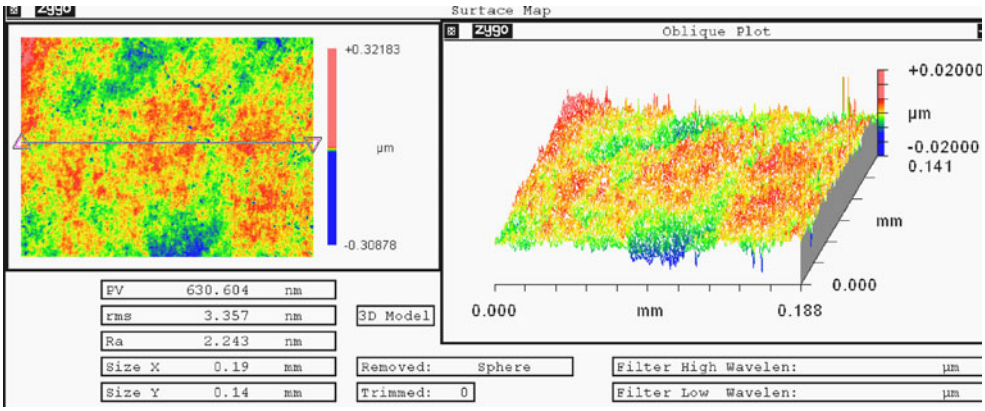

Fig. 13 Surface roughness of aspheric insert after compensation grinding

in Fig. 12. The temperature and grinding force had little effect on grinding process because of the high accuracy, high rigidity and excellent thermal stability of the machine tool. Periodic wave could be mainly attributed to the vibration possibly caused by the instability of air pressure in the wheel spindle. Nevertheless, the attenuation of periodic wave might effectively improve surface roughness and slightly for form accuracy.

The form accuracy was improved gradually with the increase of compensation cycle. Micro-topography of ground aspheric surface was shown in Fig. 13, and surface roughness of Ra 2.243 nm was obtained. To obtain a small insert with form accuracy less than PV 200 nm and nanometer surface roughness, an ultra-precision machine with nano-scale resolution and excellent thermal stability is necessary. More importantly, the optimized grinding mode and form error compensation approaches must be developed.

6 Conclusion

A single-point inclined axis grinding mode and error compensation approach were proposed for nanogrinding of small aspheric insert based on four-axis machine tools with on-machine measurement. Some conclusions are as follows:

1. To avoid interference and improve accuracy, the single-point inclined axis grinding mode is more suitable for nanogrinding small aspheric insert than arc envelope grinding.
2. By compensating the setting errors of grinding wheel, the V-shaped and Λ-shaped as well as the center navel can be obviously eliminated. Form accuracy can be further improved by adjusting the compensation ratio of form error.
3. The grinding of tungsten carbide aspheric insert demonstrated that high profile accuracy of 200 nm (in PV) with a very low roughness of 2.24 nm (in Ra) was achieved after three compensation cycles.
4. The experiment results indicate that the compensation of setting error in *X*-axis can significantly reduce the residual form error, and the residual error compensation can further improve the form accuracy.

Acknowledgments This work is sponsored by the NSFC (grant no. 50975084), the National Key Technology Program (project number 2010ZX04001-151), Young Teachers Plan of Hunan University. HH would like to acknowledge the financial support from Australian Research Council.

References

1. Ohmori H (1992) Electrolytic in-process dressing (ELID) grinding technique for ultraprecision mirror surface machining. I J JSPE 26 (4):273–278
2. Lin Y, Huang H (2008) Brittle materials in nano-abrasive fabrication of optical mirror-surfaces. Prec Eng 32:336–341
3. Chen FJ, Hu SJ, Yin SH (2012) A novel mathematical model for grinding ball end milling cutter with equal rake and clearance angle. Int J Adv Manuf Technol. doi:10.1007/s00170-011-3889-y
4. Yin SH, Morita S, Ohmori H, Uehara Y, Lin WM, Liu Q, Maihara T, Iwamuro F, Mochida D (2005) ELID precision grinding of large special Schmidt plate for fibre multi-object spectrograph for 8.2 m Subaru telescope. Int J Mach Tools Manuf 45:1598–1604
5. Ohmori H, Nakagawa T (1995) Analysis of mirror surface generation of hard and brittle materials by ELID (Electronic In-Process Dressing) grinding with superfine grain metallic bond wheels. CIRP Ann Manuf Technol 44(1):287–290
6. Chen WK, Kuriyagawa T, Huang H, Yosihara N (2005) Machining of micro aspherical mould inserts. Prec Eng 29:315–323
7. Yin SH, Ohmori H, Dai YT, Uehara Y, Chen FJ, Tang HN (2009) ELID grinding characteristics of glass–ceramic materials. Int J Mach Tools Manuf 49(3–4):333–338
8. Schmitz TL, Ziegert JC, Canning JS, Raul Z (2008) Case study: a comparison of error sources in high-speed milling. Prec Eng 32 (2):126–133
9. Nojedeh MV, Habibi M, Arezoo B (2011) Tool path accuracy enhancement through geometrical error compensation. Int J Mach Tools Manuf 51(6):471–482
10. Liang JC, Li HF, Yuan JX, Ni J (1997) A comprehensive error compensation system for correcting geometric, thermal, and cutting force-induced errors. Int J Adv Manuf Technol 13 (10):708–712

11. Lei WT, Sung MP (2008) NURBS-based fast geometric error compensation for CNC machine tools. Int J Mach Tools Manuf 48(3–4):307–319
12. Uddin MS, Ibaraki S, Matsubara A, Matsushita T (2009) Prediction and compensation of machining geometric errors of five-axis machining centers with kinematic errors. Prec Eng 33(2):194–201
13. Khan AW, Chen WY (2011) A methodology for systematic geometric error compensation in five-axis machine tools. Int J Adv Manuf Technol 53(5–8):615–628
14. Wu H, Zhang HT, Guo QJ, Wang XS, Yang JG (2008) Thermal error optimization modeling and real-time compensation on a CNC turning center. J Mater Process Technol 207(1–3):172–179
15. Creighton E, Honegger A, Tulsian A, Mukhopadhyay D (2010) Analysis of thermal errors in a high-speed micro-milling spindle. Int J Mach Tools Manuf 50(4):386–393
16. Zhang YH, Wu Q, Hu DJ (2008) Research on wear detection of wheel in precision NC curve point grinding. Int J Adv Manuf Technol 35(9–10):994–999
17. Rahman MS, Saleh T, Lim HS, Son SM, Rahman M (2008) Development of an on-machine profile measurement system in ELID grinding for machining aspheric surface with software compensation. Int J Mach Tools Manuf 48(7–8):887–895
18. Suzuki H, Tanaka K, Takeda H, Kawakami K, Nishioka M (1999) Study on precision grinding of micro aspherical surface: effects of tool errors on workpiece form accuracies and its compensation methods. J Japan Soc Prec Eng 65:401–405
19. Lee WB, Cheung CF, Chiu WM, Leung TP (2000) An investigation of residual form error compensation in the ultra-precision machining of aspheric surfaces. J Mater Process Technol 99:129–134
20. Habibi M, Arezoo B, Nojedeh MV (2011) Tool deflection and geometrical error compensation by tool path modification. Int J Mach Tools Manuf 51(6):439–449
21. Huang H, Chen WK, Kuriyagawa T (2007) Profile error compensation approaches for parallel nanogrinding of aspheric mould inserts. Int J Mach Tools Manuf 47(15):2237–2245
22. Chen FJ, Yin SH, Huang H, Ohmori H, Wang Y, Fan YF, Zhu YJ (2010) Profile error compensation in ultra-precision grinding of aspheric surfaces with on-machine measurement. Int J Mach Tools Manuf 50(5):480–486